

Model of the electron-phonon interaction and optical conductivity of $\text{Ba}_{1-x}\text{K}_x\text{BiO}_3$ superconductors

R. Nourafkan¹, F. Marsiglio², and G. Kotliar¹

¹ *Department of Physics & Astronomy, Rutgers University, Piscataway, NJ 08854-8019, USA and*

² *Department of Physics, University of Alberta, Edmonton, Alberta, Canada T6G 2E1*

We investigate the physical properties of the $\text{Ba}_{1-x}\text{K}_x\text{BiO}_3$ compounds with a focus on the optical properties. Results from the simple Holstein model, describing a single band coupled to an oxygen breathing mode with parameters derived from first principles calculations, are in excellent agreement with a broad range of experimental information. It accounts for an insulating parent compound at $x = 0$ with a direct- (optical) and an indirect-gap, and a metal insulator transition around $x = 0.38$. Strong electron-phonon coupling leads to spectral weight redistribution over a frequency scale much larger than the characteristic phonon frequency and to strongly anharmonic phonons. We find that the metallic phase in the vicinity of phase boundary is close to the polaronic regime.

PACS numbers: 74.25.Gz, 74.70.-b, 71.38.-k

Compounds of the $\text{Ba}_{1-x}\text{K}_x\text{BiO}_3$ family exhibit both superconductivity ($T_c \approx 30$ K) and an exotic semiconducting state [1–5]. The parent compound (BaBiO_3), with one valence electron per Bi atom, is an insulator. Upon substitution of Ba with K an insulator-metal transition occurs at $x \approx 0.37$. Significant effort has been made to understand optical conductivity (OC) measurements, which, in the metallic phase, display in addition to a Drude peak a substantial amount of spectral weight in the mid-infrared (MIR) frequency region [6, 7]. However, there is no consensus on the origin of the features of the OC. Interpretations have been put forward arguing in favor of very weak e-ph coupling [8–10] as well as very strong e-ph coupling, which can even be responsible for polaronic and bipolaronic behavior [5, 11–15].

In this letter we reevaluate the physical consequences of the e-ph interaction in the $\text{Ba}_{1-x}\text{K}_x\text{BiO}_3$ family, within a simple model with parameters extracted from recent electronic structure calculations [16, 17]. To solve the model we use Dynamical Mean Field Theory (DMFT) [18], with an Exact Diagonalization solver. We focus on the impact of e-ph coupling on the OC, and use comparison of theory and experiments to elucidate the strength of the e-ph coupling in this class of materials.

Band theory calculations indicate that a single anti-bonding Bi-O $sp(\sigma)$ band crosses the Fermi level [19, 20]. Furthermore, only optical phonons couple strongly to the electrons. Our central approximation is to retain the coupling to a single phonon mode, the breathing mode, and take its coupling constant to be independent of momentum (this derivation is described in the supplemental materials (SM)). This mode is most important since its condensation gives rise to the charge ordered insulating state at low filling [21]. Therefore we use a minimal single band model Hamiltonian with Holstein e-ph coupling (see SM).

A quantity of central importance is the effective e-ph coupling strength defined by the low frequency behavior of the electron self-energy. In DMFT, the effective mass of the electron is given by $m_b/m^* = (1 - \partial \text{Re} \Sigma(\omega)/\partial \omega|_{\omega=0})^{-1}$, which is related to the effective coupling, λ_{eff} , by $m^*/m_b = 1 + \lambda_{\text{eff}}$. m_b is the electronic band mass of the carriers. The

value of λ_{eff} includes phonon renormalization effects, and will generally be significantly higher than the bare coupling, λ_0 , defined as $(2g^2/\hbar\omega_0)N(\epsilon_F)$, where g is e-ph coupling constant, ω_0 is phonon frequency and $N(\epsilon_F)$ is the density of states at the Fermi level. A second way to estimate the effective or renormalized value of lambda is via the formula, $\lambda_{\text{eff}} = -g^2 N(\epsilon_F) \text{Re} D(0) = \lambda_0/(1 + 2\text{Re} \Pi(0)/\hbar\omega_0)$, where $D(\omega)$ denotes phonon propagator and $\Pi(\omega)$ is phonon self-energy. In our case the above definitions lead to the same value for λ_{eff} . It is the renormalized value of the e-ph coupling, i.e. λ_{eff} , that should be compared with experiments [22, 23].

In DMFT [18], due to the absence of vertex corrections, the OC can be expressed as a functional of the fully interacting single particle Green function, $\mathbf{G}(\epsilon_{\mathbf{k}}, \hbar\omega)$, as

$$\text{Re } \sigma_{\alpha\alpha}(\omega) = (1 + \frac{F_1}{3}) \frac{(\pi e^2/\hbar)}{V_{\text{cell}} N} \sum_{\mathbf{k}, \sigma} \int d\epsilon \frac{f(\epsilon) - f(\hbar\omega + \epsilon)}{\hbar\omega} \times \text{Tr}[\mathbf{v}_{\alpha}(\mathbf{k}) A_{\mathbf{k}\sigma}(\epsilon) \mathbf{v}_{\alpha}(\mathbf{k}) A_{\mathbf{k}\sigma}(\hbar\omega + \epsilon)], \quad (1)$$

where $A_{\mathbf{k}\sigma}(\epsilon) \equiv (-1/\pi) \text{Im} \mathbf{G}_{\sigma}(\epsilon_{\mathbf{k}}, \epsilon)$ is the interacting spectral function, $\mathbf{v}_{\alpha}(\mathbf{k}) \equiv \frac{\partial \epsilon_{\mathbf{k}}}{\partial k_{\alpha}}$, $f(\epsilon)$ is the Fermi function, and $V_{\text{cell}} = N_{\text{Bi}} a^3$ is the unit cell volume. N_{Bi} is the number of Bi ions in a unit cell. The lattice constant value is $a = 4.27 \text{ \AA}$. A Landau parameter F_1 [24] renormalizes the current operator in Eq. (1) [25].

When only intra-band optical transitions relative to the lowest conduction band contribute to the optical spectral weight (OSW), one obtains the *restricted or partial sum rule* [26]

$$W_{\text{opt}} = 2 \int_0^{\infty} d\omega \text{Re } \sigma_{\alpha\alpha}(\omega) = (1 + \frac{F_1}{3}) \frac{\pi e^2}{\hbar^2 V_{\text{cell}}} \frac{1}{N} \sum_{\mathbf{k}\sigma} n_{\mathbf{k}\sigma} \frac{\partial^2 \epsilon(\mathbf{k})}{\partial k_{\alpha}^2}. \quad (2)$$

From a knowledge of the optical spectral weight, we can calculate the plasma frequency, given by $W_{\text{opt}} = \omega_p^2/4$.

To appreciate the range of frequencies over which the optical spectral weight redistributes, it is customary to define the

effective carrier number per Bi ions participating in optical transitions, $N_{\text{eff}}(\omega)$, defined by the partial integral of the OC for frequencies less than ω as

$$\left(\frac{m_0}{m_b}\right) N_{\text{Bi}} N_{\text{eff}}(\omega) = \frac{2m_0 V_{\text{cell}}}{\pi e^2} \int_0^\omega d\nu \text{Re}\sigma_{\alpha\alpha}(\nu), \quad (3)$$

where m_0 is the free-electron mass. In order to compare the theoretical results with the experiments of Ref. [7] for $N_{\text{eff}}(\omega)$ we adopt their convention and set $m_0/m_b = 1$.

Integrating up to infinite frequency one recovers the OSW. A reduction of W_{opt} relative to its non-interacting value, as given, for example, in a LDA estimation [27], is usually taken as a sign of the presence of electron-electron correlation [28]. Before focusing on the $\text{Ba}_{1-x}\text{K}_x\text{BiO}_3$ compounds, we now revisit this issue on general grounds for the e-ph problem.

Fig. 1 (a) displays the normalized OSW in the normal and CDW phases at half-filling ($x = 0$) for a particle-hole symmetric model. The most important feature of Fig. 1 (a) is that in the weak to intermediate range of λ_0 the total OSW in a homogeneous normal metallic phase depends only weakly on the strength of the e-ph coupling as in Migdal-Eliashberg theory. The OSW reduction due to e-ph coupling is only appreciable by approaching the polaronic regime, but even upon entering that regime the OSW is substantial while the effective mass is considerably enhanced, as shown in Fig. 1 (a) and (b). These results are similar away from half-filling. Fig. 1 (b) shows the Drude part [29] normalized by the non-interacting total optical integral, $W_{\text{opt}}(g = 0)$. In our case, without any other interaction, $W_{\text{opt}}(g = 0) = W_D(g = 0)$. The $W_D(g)/W_D(g = 0)$ and inverse effective mass agree and both go continuously to zero at the critical coupling strength, $\lambda_{0c} \approx 0.455$.

Hence the variation in the Drude weight or the effective mass with e-ph coupling is more prominent than the variation in OSW. Fig. 1 (a) also shows that for $\lambda_0 < \lambda_{0c}$, ordering of itinerant carriers in a charge density wave (CDW) phase leads to a larger reduction of OSW than normal phase. However, for $\lambda_0 \geq \lambda_{0c}$, the carriers are localized in real space, due to bipolaron formation, and CDW ordering enhances OSW. Therefore, the e-ph coupling dependence of the difference between OSW in the metallic and CDW phases is not monotonic (similar to the temperature dependence of the OSW [31]).

To focus on the $\text{Ba}_{1-x}\text{K}_x\text{BiO}_3$ compounds, we determine the hopping parameters to fit the LDA band structure [19] which results in following hopping parameters $t_1 = 0.3926$, $t_2 = 0.0516$, $t_3 = -0.0017$, $t_4 = -0.0987$, all in eV. The strong energy variation of the electron DOS for the real material (see SM) leads to a strong doping dependence of the bare e-ph coupling, λ_0 , which plays a central role for understanding the physical properties of the $\text{Ba}_{1-x}\text{K}_x\text{BiO}_3$ family. For the phonon frequency and e-ph coupling we choose a set of the *bare* parameters, $\hbar\omega_0 = 80$ meV, and $g = 0.2275$ eV. The value of the e-ph coupling to the breathing mode, g , matches closely to the recent results of first principles calculation of the deformation potential at the zone boundary [17] (see SM). The characteristic phonon frequency represents a *bare* parameter. Below, we shall see that it becomes renor-

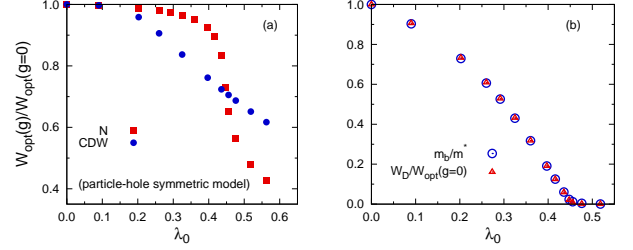


FIG. 1. (Color online) Panel(a): normalized interacting OSW as a function of bare e-ph coupling, λ_0 , at half-filling ($x = 0$) for a particle-hole symmetric model in the normal and CDW phases. Panel(b): normalized Drude weight and inverse effective mass as a function of λ_0 . The TB parameters for this figure are: $t_1 = 0.3926$ eV and $\hbar\omega_0 = 0.08$ eV.

malized, so that the final value is representative of the experimental value. For simplicity we take all the bare parameters in the Hamiltonian to be independent of doping (rigid band picture). Considering the simplifications made, our results are in surprisingly good agreement with experiments.

For the parent compound, BaBiO_3 ($x = 0$), we show the calculated conductivity as a function of frequency in panel (a) of Fig. 2, along with two measurements [6, 7] performed at room temperature. The calculated conductivity displays a characteristic insulating spectrum; the Drude peak is absent, and spectral weight has been transferred to the region above the gap. The calculated gap value, $\Delta_{\text{opt}} \approx 2$ eV, and the subsequent absorption strength are similar in magnitude to the observed values [6, 7]. The inset shows the phonon density of states in CDW phase with a renormalized peak near ≈ 72 meV, in good agreement with the experimental value of the breathing mode phonon frequency (Experimental data in [20]) [33].

In Fig. 2 (b) we show $N_{\text{eff}}(\omega)$ vs. ω for the undoped system. The calculated N_{eff} is in good agreement with the experimental data in the range of frequencies in which inter-band transitions play no role ($\omega \leq 3$ eV). Fig. 2 (c) shows the electron DOS in the charge ordered phase; it shows a gap value ≈ 0.5 eV, which corresponds to the indirect gap in BaBiO_3 [34].

Upon doping the system we find that at doping value around $x \approx 0.38$, charges distribute uniformly between the two sublattices. Investigation of the electronic DOS indicates that this is a transition to a metallic state with a finite DOS at the Fermi energy. In the intermediate doping range $0 < x < 0.38$, the electron density oscillates between two values in successive iterations of the DMFT cycle and a converged answer was not found. This implies that the system either has a tendency towards another phase, like a non-commensurate CDW, or a tendency towards phase separation, both of which cannot be seen in our study [35].

Fig. 3 (a) shows the calculated OC for two doping values in the metallic phase. As the system is doped into the metallic phase, the optical response shows a Drude peak, cen-

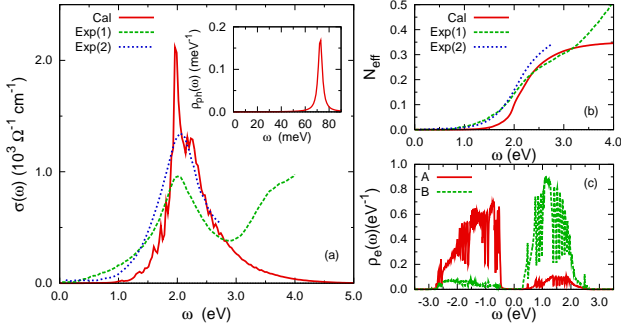


FIG. 2. (Color online) (a) Calculated and measured OC at half-filling ($x = 0$). Measured OCs of BaBiO_3 are reproduced from [6, 7], labeled by (1) and (2), respectively. Inset: The renormalized phonon density of states. (b) Calculated and measured effective carrier number per Bi ion participating in the optical transitions. (c) Electron DOS in the charge ordered phase with an indirect gap of the order of $\Delta \approx 0.5$ eV. A and B indicate the majority and minority sublattices for electron density.

tered at $\omega = 0$. This indicates coherent quasi-particle motion, and an additional mid-infrared (MIR) feature arises, caused by single- and multi-phonon excitations and absorption processes. The MIR contribution is an incoherent component of the OC, and corresponds to optical transitions in which the carrier is excited but leaves behind a local distortion, which corresponds to real excitations. This MIR component occurs at frequencies characteristic of these excitations. As we saw in Fig. 1 (b), the e-ph interaction causes a reduction of the free carrier Drude peak weight; in fact it is approximately reduced by the quasi-particle renormalization factor $(1 + \lambda_{\text{eff}})^{-1}$ and the spectral weight increases in the MIR energy range reflecting the incoherent scattering excitations that result from absorption processes assisted by the e-ph interaction. The MIR frequency range extends well beyond that of the characteristic phonon frequency.

In the inset of Fig. 3 we show the effective carrier number calculated from OC. In the metallic phase $N_{\text{eff}}(\omega)$ at first increases steeply at low frequencies, on account of the appearance of the Drude band centered at $\omega = 0$, and continues to increase in the mid-infrared region, eventually saturating at a high frequency. The trends are in good agreement with the experimental data [7, 36].

Fig. 3 (b) shows the phonon density of states. The bare phonon frequency is softened and the phonon DOS shows structures similar to those observed experimentally [32]. The effective oscillator potential and anharmonicity is further explored in the SM. Consistent with experimental results [37], the effective potential shows a double well structure, with one minimum disappearing with increased doping.

We now turn to the doping dependence of the OSW. Due to a higher value of the DOS at ($x = 0$) the e-ph coupling (λ_0) is largest in the parent compound and decreases with doping. Fig. 3 (c) shows the normalized interacting OSW vs. doping. It is clear that the OSW is greatly reduced for small values of

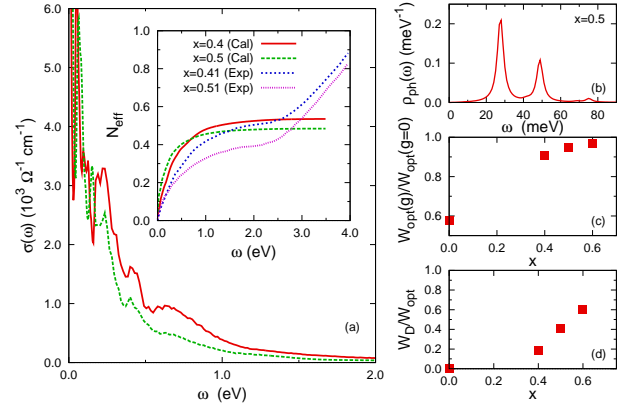


FIG. 3. (Color online) (a) Calculated and experimental [7] conductivity for the indicated doping x at zero temperature. Inset: Effective carrier number participating in the OC as a function of frequency. (b) The phonon density of states at $x = 0.5$. (c) Normalized interacting OSW by non-interacting value as a function of doping. (d) Drude weight, W_D , of the OC, normalized by total weight W_{opt} , as a function of the doping level. In panels (c) and (d), system at $x = 0$ is in CDW phase, while other data points show normal metallic phase.

x due to the e-ph interaction. In the metallic phase, upon increasing the doping level, electrons become more undressed, which leads to a smaller optical weight reduction.

Fig. 3 (d) shows the Drude part (the MIR part is $W_{\text{opt}} - W_D$) normalized by the total optical integral as a function of doping at $T = 0$ [38]. In the metallic phase the OSW redistributes between the Drude peak and the MIR shoulder, and by increasing the doping level the Drude weight rises very quickly. For instance, the Drude peak weight increased by almost a factor of two with increasing x from $x = 0.4$ to $x = 0.5$.

In the DMFT framework, the effective e-ph coupling can be extracted either from the phonon propagator at zero frequency, or the effective mass, or from the relative weight of the Drude peak to the total OSW in the absence of e-ph coupling, $W_D(g)/W_{\text{opt}}(g = 0) \approx (1 + \lambda_{\text{eff}})^{-1}$. We found that the effective e-ph coupling is strongly doping dependent with the highest value ($\lambda_{\text{eff}} \geq 4$) at $x = 0.4$ close to the transition to the insulating phase. With such a high value of the effective e-ph coupling the formation of an inhomogeneous phase in the vicinity of the phase boundary is highly likely. At higher doping levels where the system is likely to be homogeneous, we find $\lambda_{\text{eff}} \approx 1.6$ for $x = 0.5$.

The calculated plasma frequency for $x = 0.5$ is $\hbar^2 \omega_p^2 = 8.95 \text{ eV}^2$, again in good agreement with the experimental value [15]. Using the calculated values for the plasma frequency for $x = 0.5$ we can use the high temperature behavior of the measured resistivity to estimate the e-ph coupling, $\lambda_{\text{eff}}^{(\text{tr})}$ [39]. Using the high temperature resistivity formula [14],

$$\rho(T) \approx \rho_{\text{ph}}(T) \approx \frac{8\pi^2 k_B}{\hbar} \frac{\lambda_{\text{eff}}^{(\text{tr})}}{\omega_p^2} T \quad (4)$$

we estimate a value of $\lambda_{\text{eff}}^{(\text{tr})} \approx 1.75$.

In support of strong e-ph coupling, heat capacity measurements for $\text{Ba}_{1-x}\text{K}_x\text{BiO}_3$ with $x \approx 0.4$ show a jump in the specific heat of the order $\Delta C_p(T_c)/T_c \approx 4 - 5 \text{ mJ mol}^{-1}\text{K}^{-2}$ at T_c [40]. One can relate this to the coefficient of the electronic specific heat, γ , by the BCS expression $\Delta C_p(T_c)/T_c = 1.43\gamma$ [41]. Then from the relation $\gamma = (2/3)\pi^2 N(\epsilon_F)k_B^2(1 + \lambda_{\text{eff}})$ with use of $N(\epsilon_F) = 0.23 \text{ states/eV spin cell}$ for $x = 0.5$, λ_{eff} is estimated to be $1.6 - 2.2$, consistent with our previous estimates.

In conclusion we have revisited the physical properties of $\text{Ba}_{1-x}\text{K}_x\text{BiO}_3$, using a model Hamiltonian with parameters inspired by recent first principles calculations [16, 17] but going beyond these calculations by taking into account the full many body physics and inherent anharmonicity of a strongly coupled e-ph system. For small doping the coupling is strong enough to sustain polaron and small bipolaron formation and the coupling decreases for large doping. For the metallic regime near the phase transition boundary, we find a situation intermediate between a Fermi/BCS liquid and a bipolaronic superconductor, in agreement with experimental studies [42, 43]. The model accounts for experimentally determined gaps (both direct and indirect) in the parent compound at $x = 0$ and an abrupt insulator transition at a critical doping. In the metallic phase, we find a strongly anharmonicity in agreement with recent experiments [37] and transfer of substantial electron phonon coupling strength to low frequencies as shown in the phonon density of states. Strong e-ph coupling reduces the width of the Drude peak and transfers spectral weight to the mid-infrared structure. Spectral weight redistributes over a frequency scale that is much larger than the phonon frequency. Further extensions will require the incorporation of couplings to other phonon modes and of additional bands in the modeling. These are not expected to change drastically the main conclusions presented in this paper which focused on the electronic properties but are certainly required for a more realistic study of the phonon spectra.

Acknowledgments. This research was supported by the AFOSR MURI Towards New and Better High Temperature Superconductors. GK is grateful to Dimitri Basov for useful discussions. RN and GK would like to thank Zhiping Yin for many helpful discussion. FM acknowledges support by the Natural Sciences and Engineering Research Council of Canada (NSERC). FM and GK acknowledge the support of the Canadian Institute for Advanced Research (CIFAR).

[1] R. J. Cava, *et al.*, Nature (London) **332**, 814 (1988).
 [2] A. W. Sleight, J. G. Gillson, P. E. Bierstedt, Solid State Commun. **17**, 27 (1975).
 [3] C. M. Varma, Phys. Rev. Lett. **61**, 2713 (1988).
 [4] T. M. Rice and L. Sneddon, Phys. Rev. Lett. **47**, 689 (1981).
 [5] I. B. Bischofs, V. N. Kostur, and P. B. Allen, Phys. Rev. B **65**, 115112 (2002).

[6] S. H. Blanton, R. T. Collins, K. H. Kelleher, L. D. Rotter, Z. Schlesinger, D. G. Hinks and Y. Zheng, Phys. Rev. B **47**, 996 (1993).
 [7] M. A. Karlow, S. L. Cooper, A. L. Kotz, M. V. Klein, P. D. Han and D. A. Payne, Phys. Rev. B **48**, 6499 (1993).
 [8] A. V. Puchkov, T. Timusk, W.D. Mosley and R.N. Shelton, Phys. Rev. B **50** 4144 (1994).
 [9] F. Sharifi, A. Pargellis, R.C. Dynes, B. Miller, E.S. Hellman, J. Rosamilia, and E.H. Hartford, Jr. Phys. Rev. B **44**, 12521 (1991).
 [10] F. Marsiglio, J.P. Carbotte, A. Puchkov and T. Timusk, Phys. Rev. B **53**, 9433 (1996).
 [11] M. Merz *et al.*, Europhys. Lett. **72** 275 (2005).
 [12] A. V. Puchkov, T. Timusk, M. A. Karlow, S. L. Cooper, P. D. Han and D. A. Payne, Phys. Rev. B **54**, 6686 (1996).
 [13] Q. Huang, *et al.*, In: *Electron-Phonon Interaction in Oxide Superconductors*, edited by R. Baquero (World Scientific, Singapore (1991)), p. 46.
 [14] N. Tralshawala, *et al.*, Phys. Rev. B **51**, 3812 (1995).
 [15] E. S. Hellman and E. H. Hartford, Jr., Phys. Rev. B **47**, 11346 (1993).
 [16] C. Franchini, G. Kresse, R. Podloucky, Phys. Rev. Lett. **102**, 256402 (2009).
 [17] Z. P. Yin, A. Kutepov, and G. Kotliar, arXiv:1110.5751.
 [18] A. Georges, G. Kotliar, W. Krauth and M. J. Rozenberg, Rev. Mod. Phys. **68** 13 (1996).
 [19] L. F. Mattheiss and D. R. Hamann, Phys. Rev. B **28**, 4227 (1983).
 [20] V. Meregalli and S. Y. Savrasov, Phys. Rev. B **57**, 14453 (1998).
 [21] K. Inumaru, H. Miyata, and S. Yamanaka, Phys. Rev. B **78**, 132507 (2008).
 [22] F. Marsiglio, Phys. Rev. B **42**, 2416 (1990).
 [23] J. Bauer, J. E. Han, and O. Gunnarsson, Phys. Rev. B **84**, 184531 (2011).
 [24] A. J. Millis, In: *Strong Interactions in Low Dimensions*, D. Baeriswyl and L. DeGiorgi, eds (Springer Verlag: Berlin 2004).
 [25] The introduction of the F_1 can be motivated as follows; Hybrid density functional theory contains about twenty to thirty percent exchange contributions to the band dispersions, but exchange contributions should not contribute to the current via the Peierls substitution. We incorporate this effect via a Landau coefficient $(1 + F_1/3)$ multiplying the Peierls expression relating the current to the derivative of the energy dispersion with respect to momentum. We adopt a value of $1 + F_1/3 = 0.8$, removing twenty percent of the current originating from the exchange term in the self energy.
 [26] P.F. Maldague, Phys. Rev. B **16**, 2437 (1977).
 [27] The HSE values for optical spectral weights in the metal are close to the LDA value.
 [28] D. N. Basov, and T. Timusk, Rev. Mod. Phys. **77**, 721 (2005).
 [29] The Drude weight, W_D , is determined by examining the asymptotic form of the current-current susceptibility on the imaginary axis [30].
 [30] D. J. Scalapino, S. R. White, S. Zhang, Phys. Rev. B **47**, 7995 (1993).
 [31] S. Ciuchi, and S. Fratini, Phys. Rev. B **77**, 205127 (2008).
 [32] Q. Huang *et al.*, Nature (London) **347**, 369 (1990).
 [33] The e-ph coupling in the parent compound is sufficiently strong to cause real-space pairing of carriers in the form of small bipolarons; however, this phase is hidden by the charge ordered phase.
 [34] H. Takagi *et al.*, in 18th Int. Conf. on the Physics of Semiconductors, edited by O. Engstrom (Singapore: World Scientific, Stockholm, 1987), pp. 1851-1855.
 [35] J. K. Freericks and M. Jarrell, Phys. Rev. B **50**, 6939 (1994).

- [36] Indeed, upon increasing the doping level one expects that $(m_0/m_b)N_{\text{eff}}(\omega_c)$ gets closer to the expected carrier number determined from the chemical composition $1 - x$. Here, $\hbar\omega_c$ is a cutoff energy which must be chosen to exhaust the oscillator strength of the absorption in question but lie below the rest of the absorption bands. Assuming a small variation in (m_0/m_b) between $x = 0.4 - 0.5$, then the difference between $N_{\text{eff}}(\omega_c)$ and $1 - x$ decreases upon increasing the doping level. Our calculations show this behavior. While the early experimental data of Ref. [7] shows the opposite trend, later observation shows a trend consistent with our calculated results [12].
- [37] A. P. Menushenkov and K. V. Klementev, J. Phys.: Condens. Matter **12**, 3767 (2000).
- [38] The total weight, W_{opt} , determined by summing the area under the conductivity, agrees with the calculated partial sum rule, which is an independent calculation (right hand side of Eq. (2)), and confirms the sum rule.
- [39] The superscript 'tr' is for transport properties. For our purposes we will regard this as equivalent to the effective coupling strength defined through the effective mass.
- [40] S. Blanchard *et al.*, Phys. Rev. Lett. **88**, 177201 (2002).
- [41] This value is higher for stronger electron-phonon interaction — see, for example, F. Marsiglio and J.P. Carbotte, Phys. Rev. **33**, 6141 (1986), but the BCS value will serve as an estimate.
- [42] Y. J. Uemura *et al.*, Phys. Rev. Lett. **66**, 2665 (1991).
- [43] C. C. Homes, Physica C **445-448**, 8 (2006).

Model of the electron-phonon interaction and optical conductivity of $\text{Ba}_{1-x}\text{K}_x\text{BiO}_3$ superconductors - Supplemental materials

I. ELECTRON-PHONON COUPLING

Here we provide additional information on the derivation of a Holstein-type e-ph coupling from the Rice-Sneddon model Hamiltonian [1]. The phonon part and e-ph interaction in the Rice-Sneddon model Hamiltonian is given by

$$H_{ph} + H_{e-ph} = \frac{M_O}{2} \sum_{i\alpha} (\dot{u}_{i\alpha}^2 + \omega_0^2 u_{i\alpha}^2) - \mathcal{G} \sum_{i\alpha} n_i (u_{i\alpha+} - u_{i\alpha-}) \quad (\text{S1})$$

where $u_{i\alpha\pm}$ denote displacements of two oxygen ions at sites $\mathbf{R}_i \pm a\hat{\mathbf{e}}_\alpha/2$, placed in the α th direction at a distance $a/2$, and \mathcal{G} is the strength of this interaction. M_O is the oxygen ion mass, and ω_0 is the phonon frequency.

Introducing the boson representation for each oxygen coordinate, $u_{i\alpha} = \sqrt{\hbar/2M_O\omega_0}(B_{i\alpha}^\dagger + B_{i\alpha})$, Eq. (S1) reads

$$H_{ph} + H_{e-ph} = \hbar\omega_0 \sum_{i\alpha} (B_{i\alpha}^\dagger B_{i\alpha} + \frac{1}{2}) - \mathcal{G} \sqrt{\frac{\hbar}{2M_O\omega_0}} \sum_{i\alpha} n_i [(B_{i\alpha+}^\dagger - B_{i\alpha-}^\dagger) + h.c.]. \quad (\text{S2})$$

With these phonon coordinates, being attached to oxygen ions, there is a nonzero overlap between nearest-neighbor operators, i.e., they are not orthogonal. It is better to define new orthogonal boson operators [2]. By Fourier transforming the boson operators, $B_{i\alpha\pm} = (1/\sqrt{N}) \sum_{\mathbf{k}} \exp[i\mathbf{k} \cdot (\mathbf{R}_i \pm a\hat{\mathbf{e}}_\alpha/2)] B_{\mathbf{k}\alpha\pm}$, it is easy to show

$$H_{e-ph} = -\frac{2\mathcal{G}}{\sqrt{N}} \sqrt{\frac{\hbar}{2M_O\omega_0}} \sum_i n_i \sum_{\mathbf{k}} \mu_{\mathbf{k}} (e^{i\mathbf{k} \cdot \mathbf{R}_i} b_{\mathbf{k}}^\dagger + h.c.), \quad (\text{S3})$$

where N is the number of sites, $b_{\mathbf{k}}$ represents a symmetric phononic mode

$$b_{\mathbf{k}} = -\frac{i}{\mu_{\mathbf{k}}} \sum_{\alpha} B_{\mathbf{k}\alpha} \sin \frac{k_{\alpha}}{2}, \quad (\text{S4})$$

and

$$\mu_{\mathbf{k}} = \sqrt{\sin^2(k_x/2) + \sin^2(k_y/2) + \sin^2(k_z/2)}. \quad (\text{S5})$$

The new operators, $b_{\mathbf{k}}$, fulfill the boson commutation relations. By transforming the new operator back to real space we obtain the following form of the phonon related terms

$$H_{ph} + H_{e-ph} = \hbar\omega_0 \sum_i (b_i^\dagger b_i + 1/2) - \sum_{ij} g_{ij} n_i (b_j^\dagger + b_j) \quad (\text{S6})$$

where $g_{ij} = 2\mathcal{G}\sqrt{\hbar/2M_O\omega_0}\gamma_{ij}$. The coefficients $\gamma_{ij} = \frac{1}{\sqrt{N}} \sum_{\mathbf{k}} \mu_{\mathbf{k}} \exp[-i\mathbf{k} \cdot (\mathbf{R}_i - \mathbf{R}_j)]$ are responsible for the long-range e-ph interaction, which is a consequence of orthogonalization of the local phonon modes. However, these terms fall off rapidly with distance (e.g. $\gamma(0) = 1.19$, and $\gamma(1) = -0.11$) [2]. In the Holstein model, we only keep the first term $g \equiv g_{ii} = 2\mathcal{G}\sqrt{\hbar/2M_O\omega_0}\gamma(0)$. Therefore, we use following model Hamiltonian:

$$H = - \sum_{i,j,\sigma} t_{ij} (c_{i\sigma}^\dagger c_{j\sigma} + h.c.) + g \sum_i (n_i - 1)(b_i + b_i^\dagger) + \hbar\omega_0 \sum_i b_i^\dagger b_i, \quad (\text{S7})$$

where $c_{i\sigma}$ ($c_{i\sigma}^\dagger$) and b_i (b_i^\dagger) are the destruction (creation) operators for electrons with spin σ and local vibrons with frequency ω_0 , respectively. The operator $n_i \equiv \sum_{\sigma} c_{i\sigma}^\dagger c_{i\sigma}$ is the electron density at site i , the parameters t_{ij} are the electron hopping matrix elements between sites i and j , and g denotes the e-ph coupling constant.

Using $\hbar\omega_0^{\text{LDA}} = 0.065$ eV, and $\mathcal{G} = \mathcal{D}^{\text{LDA}}/6$ the value of g would be $g = 0.237$ eV. Here $\mathcal{D}^{\text{LDA}} = 13.3$ eV \AA^{-1} is the deformation potential obtained from the LDA calculation [3].

The displacement of the oxygen ion is approximately given by $u_{i\alpha} \approx (1/3)\sqrt{\hbar/2M_O\omega_0}\gamma(0)\langle b_i + b_i^\dagger \rangle$. Our model Hamiltonian calculation, with $\hbar\omega_0 = 0.08$ eV, gives a value $\langle b_i + b_i^\dagger \rangle \approx 4.5$ for the undoped case, which leads to a breathing mode distortion of the order of $u_i \approx 0.073 \text{\AA}$, in agreement with the experimental value 0.085\AA [4].

II. DENSITY OF STATES

In Fig. S1 we show the resulting density of state (DOS) for a specific choice of hopping parameters $t_1 = 0.3926$, $t_2 = 0.0516$, $t_3 = -0.0017$, $t_4 = -0.0987$, all in eV (TB1). These correspond to successively further neighbor hopping. Note the appearance of a (diverging) van Hove singularity, the result of including beyond nearest neighbor hopping, and in strong contrast to the rather flat DOS for the nearest neighbor model (TB2). The strong energy variation of the electron DOS for the real material leads to a strong doping dependence of the bare e-ph coupling, λ_0 , which plays a central role for understanding the physical properties of the $\text{Ba}_{1-x}\text{K}_x\text{BiO}_3$ family.

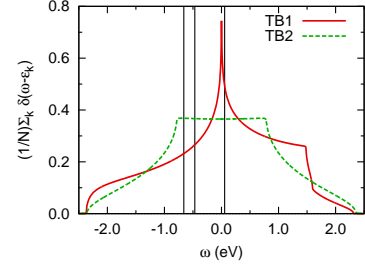


FIG. S1. (Color online) The density of states of the tight-binding model (TB1). Note the van Hove singularity. Vertical lines indicate the non-interacting chemical potential for $x = 0.5$, $x = 0.4$ and $x = 0$. Also shown is the DOS for nearest neighbor hopping only (TB2).

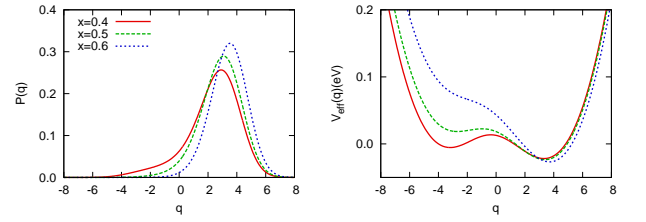


FIG. S2. (Color online) The phonon displacement probability-distribution function (left panel) and the effective phonon potential (right panel) for three different doping levels.

III. EFFECTIVE PHONON POTENTIAL

In an electron-phonon system, an effective phonon potential, V_{eff} , can be defined using an effective wavefunction defined by $\psi_{\text{eff}}(q) = \sqrt{P(q)}$, which is taken to be a solution of the one dimensional Schrodinger equation [5],

$$-\hbar\omega_0 \frac{d^2 \psi_{\text{eff}}(q)}{dq^2} + V_{\text{eff}}(q) \psi_{\text{eff}}(q) = E \psi_{\text{eff}}(q), \quad (\text{S8})$$

where $\hat{q} \equiv b + b^\dagger$ and $P(q) = \langle \phi_0 | q \rangle \langle q | \phi_0 \rangle$ is the phonon displacement probability-distribution function (PDF) [6]. The wave function $|\phi_0\rangle$ is the ground-state wave function and $|q\rangle\langle q|$ is the projection operator onto the subspace where the phonon displacement operator, \hat{q} , at a given site has value q . This quantity is a measure of the distribution of the local distortions. Having $P(q)$, the effective phonon potential $V_{\text{eff}}(q)$ is given by

$$V_{\text{eff}}(q) = E + \frac{\hbar\omega_0}{2} \left(\frac{P''(q)}{P(q)} - \frac{1}{2} \left(\frac{P'(q)}{P(q)} \right)^2 \right). \quad (\text{S9})$$

In Fig. S2 we show results for the probability distribution function and corresponding effective potential as deduced from Eq. (S9) for three different doping levels (we ignore the constant E , so we only discuss the variation in the shape

of the potential and not its absolute value). In each case $P(q)$ has a narrow peak which shifts to slightly larger q with increasing doping. The average value of the displacement, $\langle q \rangle = \int_{-\infty}^{\infty} dq \, q P(q)$, agrees with a direct calculation of $\langle b + b^\dagger \rangle$ and is given by $-(2g^2/\hbar\omega_0)(\langle n \rangle - 1)$ [5]. The effective phonon potential shows an asymmetric double well structure, with one of the minima disappearing with increased doping. Near the lowest doping value ($x = 0.4$), the potential exhibits pronounced anharmonicity, which eventually decreases as the doping increases. For the highest doping level, the shallow minimum has disappeared, and fluctuations decrease, indicated by the presence of a single minimum in the effective

potential. The enhanced fluctuations near the instability point are a signal that an instability is imminent.

- [1] T. M. Rice and L. Sneddon, Phys. Rev. Lett. **47**, 689 (1981).
- [2] P. Piekarz, J. Konior, Physica C **329**, 121 (2000).
- [3] Z. P. Yin, A. Kutepov, and G. Kotliar, arXiv:1110.5751.
- [4] D. E. Cox and A. W. Sleight, Solid State Communications **19**, 969 (1976).
- [5] A. C. Hewson and J. Bauer, J. Phys.: Condens. Matter **22** 115602 (2010).
- [6] M. Capone, P. Carta, S. Ciuchi, Phys. Rev. B **74**, 045106 (2006).